TELKOMNIKA Telecommunication, Computing, Electronics and Control
Vol. 23, No. 4, August 2025, pp. 918∼931
ISSN: 1693-6930, DOI: 10.12928/TELKOMNIKA.v23i4.26822

Energy scavenging-aided NOMA uplink communications: performance analysis

Huu Q. Tran[1], Khuong Ho-Van[2]
[1]Faculty of Electronics Technology, Industrial University of Ho Chi Minh City, Ho Chi Minh City, Vietnam
[2]Faculty of Electrical and Electronics Engineering, Ho Chi Minh City University of Technology (HCMUT), VNU-HCM, Ho Chi Minh City, Vietnam

Article Info

Article history:

Received Dec 5, 2024
Revised Apr 12, 2025
Accepted May 27, 2025

Keywords:

Nonorthogonal multiple access
Outage probability
Shadowed fading
Throughput
Uplink communications

ABSTRACT

Energy scavenging-aided nonorthogonal multiple access (NOMA) networks significantly ameliorate energy-and-spectral efficiencies thanks to superimposing a multitude of user signals for concurrent transmission and harvesting radio frequency energy. Practically, energy harvesters possess non-linear characteristic and their efficiency is enhanced considerably with deployment of multiple antennas. Moreover, communication reliability and harvested energy are directly influenced by wireless propagation which induces simultaneous effects of shadowing, path loss, and fading. Accordingly, the current paper assesses analytically outage probability and throughput of energy scavenging (ES)-aided NOMA uplink communications (eNOMAu) taking into account the above-addressed realistic factors ($\kappa - \mu$ shadowed fading, multi-antenna deployment, ES non-linearity). The results reveal considerable performance degradation caused by ES non-linearity and wireless propagation. Additionally, desired system performance can be reached flexibly with appropriate specification selection. In addition, accreting a quantity of antennas drastically mitigates the outage probability of eNOMAu, which can be minimized with optimal ES time selection. Furthermore, the proposed eNOMAu is considerably superior to its eOMAu counterpart.

Corresponding Author:

Huu Q. Tran
Faculty of Electronics Technology, Industrial University of Ho Chi Minh City
Go Vap District, Ho Chi Minh City,Vietnam
Email: tranquyhuu@iuh.edu.vn

1. INTRODUCTION

5G/6G systems grant a multitude of emerging wireless applications for a massive number of devices but enforce serious challenges on telecommunication infrastructure, particularly in current scenarios of spectrum and energy shortages, to supply sufficiently spectrum and energy for these devices [1], [2]. Therefore, solutions for improving energy and spectral efficiencies are essential and urgent.

Nonorthogonal multiple access (NOMA), which was recommended for 5G/6G networks, is a feasible solution to ameliorate spectral efficiency [3]. By distributing distinct power levels to diverse users, NOMA exploits efficiently successive decoding in combination with interference cancellation to further mitigate system outage. Furthermore, harvesting radio frequency energy present in wireless signals by NOMA users can be considered as a helpful solution in meliorating energy efficiency. Notably, an implementable ES circuit is deployed in 5G/6G transceivers [4]. Notwithstanding, a majority of performance analyses pertinent to ES have characterized ES to be linear for tractability [5]. Realistically, ES circuit is implemented by nonlinear elements, namely capacitors, inductors, diodes. Thereby, characterizing energy harvesting ought to take the non-linearity of circuit elements into account. So far, various non-linear energy harvesting models have modelled such non-linearity [3], [6], [7].

Energy scavenging-aided NOMA uplink communications (eNOMAu), viz. Figure 1, enables two NOMA transmitters (U1 and U2) to concurrently send their data to the same receiver (NR) and to scavenge energy from a power source (PS) for their transmission wherein high-and-stable power television/radio broadcasting transmitters can play a role as PS. To further ameliorate energy harvesting efficiency, PS should employ multiple antennas, which is the case in this paper.

Wireless propagation causes a multitude of impairments like path loss, fading, shadowing, which influence drastically reliability of wireless transmission. For eNOMAu under consideration in this work, wireless channels impact an amount of scavenged energy and communication reliability. For performance assessment realistically, wireless propagation must be characterized properly to fit real-world data. $\kappa - \mu$ shadowed fading paradigm is widely acknowledged to feature appropriately concurrent effects of fading, path loss, shadowing [8].

In summary, eNOMAu exposes advantages of high spectrum and energy efficiencies. Notwithstanding, the outage probability of eNOMAu is impacted by numerous real-world impairments such as wireless channel (path loss, shadowing, fading), ES non-linearity, and multi-antenna deployment. Thence, performance assessment of eNOMAu is essential to confirm whether eNOMAu possesses such superiority as working in such impairments. This paper proposes outage probability and throughput assessment under consideration of all these factors.

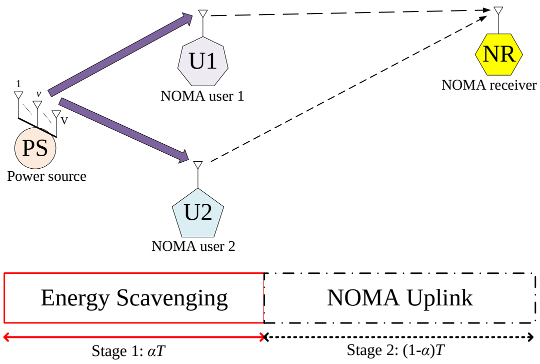

Figure 1. Energy scavenging-aided NOMA uplink communications in this paper

Wang and Men [3], eNOMAu was studied whereby multiple NOMA terminals that broadcast information to a common receiver NR need two stages (Figure 1). In stage 1, NOMA terminals utilize nonlinear energy harvesters (NLEHs) to harvest radio frequency energy from a stable PS while in stage 2, they use harvested energy to send data to NR. Wang and Men [3] showed each stage is optimized for the best performance. Nonetheless, Wang and Men [3] overlooked the explicit analysis of secrecy outage probability. The particular example of [3] with two NOMA terminals was demonstrated in [9] that presented approximated outage probability analysis. Researchers [10]-[12] studied energy scavenging-aided NOMA downlink communications (eNOMAd) in which NR sends information using NOMA to two receivers (U1 and U2). Afterwards, Le *et al.* [13] performed an extension of [10]-[12] to multiple receivers. Researchers [10]-[13] derived the approximated formulas of outage probability (OP) and throughput (TP). In addition, Le *et al.* [13] maximized sum-rate. However, researchers in [10], [11], the single-antenna NOMA device provides energy for NR. In contrast, Le *et al.* [13] the multi-antenna NOMA device supplies energy for NR. Nevertheless, researchers [10], [11], [13] utilizes unrealistic linear energy harvester (LEH). Furthermore, U1 harvests radio frequency energy from the single-antenna NR by NLEH in [12].

eNOMAd with two recipients (U1 and U2) was investigated whereby transmission to U1 is aided by a relay in [14]-[16] and by U2 in [17]-[21]. The relay and U2 in [14]-[21] scavenge power from the NOMA transmitter. Researchers [16], [17] studied NLEH at the relay in their approximated OP analysis. In the meantime, researchers [14], [19], [20] solved the aggregate capacity optimization problem. Nevertheless, Liu *et al.* [14] considered LEH whereas Si *et al.* [19] and Garcia *et al.* [20] implemented NLEH. Researchers in [22], [23] performed an extension of [16] to multiple relays as well as selected the best relay to aid NOMA transmission from NR to U1 and U2. Furthermore, Zhai *et al.* [24] extended Agrawal *et al.* [16] to assist U2 by utilizing two relaying devices. However, Zhai *et al.* [24] overlooked the closed-form TP analysis. Instead of employing a multitude of relays in [22], [23], [25] exploited a multitude of near NOMA terminals and performed selecting solely one near NOMA terminal to help the far NOMA terminal. Another extension of Agrawal *et al.* [16] is to investigate several receivers in [26], [27]. Notwithstanding, researchers [15], [18], [21]-[27] conducted performance analysis for LEH. Moreover, researchers [28]-[30] exploited reconfigurable intelligent surface to relay messages from NR to U1 and U2 in order to maximize aggregate capacity. However, Lyu et al. [28] considered NLEH whereas [29], [30] investigated LEH. Additionally, system performance was not analyzed in [14], [19], [20], [28]-[30].

To sum up, the aforementioned publications pertinent to performance analysis in [3], [9]-[13], [15]-[26], [29], [30] investigated a trivial system model with the single-antenna PS, thence barely meliorating ES efficiency. Merely Aldababsa and Basar [27] studied several antennas employed at all users. Additionally, only trivial fading models without shadowing such as Rayleigh ([3], [12], [13], [16]-[21], [24], [25], [29]), Rician ([14], [15], [28], [30]), Weibull [26], Nakagami-m ([10], [11], [22], [23], [27]) have been considered in the previous publications. Thence, the updated publications overlooked the OP/TP analyses for the configuration in Figure 1 when considering path loss, shadowing, generalized $\kappa-\mu$ fading, and several antennas at PS such that U1 and U2 harvest more energy, ultimately ameliorating system performance at NR. This paper pioneers in carrying out such an analysis that is useful in evaluating swiftly and maximizing system performance prior to practical deployment.

The contributions are itemized to be: (i) we recommend eNOMAu in Figure 1 in which the arbitrary number of antennas can be deployed at PS for ameliorating energy harvesting efficiency, eventually improving system performance; (ii) to evaluate communication reliability promptly, we perform the OP/TP analyses for the proposed eNOMAu considering the non-linearity of energy harvesting, the multiple antenna consideration, and different channel impairments like path loss, fading, shadowing; and (iii) we rate and maximize system performance in distinct realistic scenarios. Multiple results demonstrate a considerable performance degradation owing to non-linearity of energy scavengers and impairments of wireless propagation. Moreover, communications reliability of eNOMAu can be controlled and maximized by adopting appropriately and flexibly several specifications. Additionally, accreting a quantity of antennas improves significantly system performance. Further, the proposed eNOMAu is considerably superior to its eOMAu counterpart.

Section 2 explains the recommended eNOMAu. Subsequently, section 3 carries out the OP and TP analyses. Then, section 4 presents the asymptotic performance analysis in the regime of high transmit power. Next, section 5 analyzes the benchmark eOMAu scheme for convenience in comparing with the proposed eNOMAu. Then, section 6 discusses simulated/analytical results in different practical settings. Eventually, section 7 concludes the paper. Notable symbols are presented in Table 1.

Table 1. Notable symbols

Symbol	Interpretation
$\mathsf{N}(0, b)$	Zero-mean and b-variance complex Gaussian random variable
$\Gamma(\cdot)$	Complete gamma function
$\mathsf{F}_Q(\cdot)$	Cumulative distribution functon (CDF) of Q
$\Pr\{\cdot\}$	Probability operator
$\bar{\mathsf{F}}_Q(\cdot)$	Complementary cumulative distribution function (CCDF) of Q
$\mathsf{E}\{\cdot\}$	Expectation operator
$\mathsf{f}_Q(\cdot)$	Probability density function (PDF) of Q
$\Theta_Q(\cdot)$	Moment generating function (MGF) of Q
$\Gamma(\cdot,\cdot)$	Incomplete upper gamma function
$\mathsf{C}_k^l = \frac{k!}{l!(k-l)!}$	Binomial coefficient

2. ENERGY SCAVENGING-AIDED NOMA UPLINK COMMUNICATIONS

2.1. System model

Figure 1 depicts eNOMAu comprising U2, U1, NR, PS. eNOMAu exemplifies uplink communications in mobile wireless systems. U2 and U1 have power limitation. Thereby, they ought to scavenge power from PS. In eNOMAu, PS provides power for operations of U2 and U1 in αT time unit of Stage 1 wherein T

mentions the frame duration and $\alpha \in (0,1)$ means the time splitting parameter, whereas U2 and U1 conduct uplink communications using NOMA to NR in the remainder of T in stage 2. To ameliorate energy scavenging efficiency, ultimately enhancing system performance, V antennas are supposed to be deployed at PS, which is possible for high-energy PS. More particular, multi-antenna PS enables U2 and U1 to scavenge energy effectively. Nonetheless, U1, U2 and NR may be mobile terminals and thence, assumption of single antenna deployed at them is more appropriate.

2.2. Channel model

Our work represents $g_{s_v i}$ and g_i correspondingly as channel gains from the v^{th} antenna of PS to Ui and from Ui to NR where $i = \{1, 2\}$. It also supposes block frequency non-selective $\kappa - \mu$ shadowed fading links. In particular, a cluster of specifications $(\mu, \kappa, \beta, \vartheta_{xy})$ determines definitely g_{xy} with $xy = \{s_v i, i\}$. In other words, by changing a parameter set $(\kappa, \mu, \beta, \vartheta_{xy})$ of such $\kappa - \mu$ shadowed fading model, one can control flexibly different impairment levels of shadowing, path loss, fading. The parameter $\vartheta_{xy} = \mathsf{E}\{g_{xy}\}$ represents channel power, which comprises path loss, μ notates the quantity of multi-path groups, β indicates shadowing effect, κ indicates the Rician-K parameter. Accordingly, this model characterizes a majority of practical wireless channels. As per [8], the PDF and CDF of g_{xy} are given by

$$\mathsf{f}_{g_{xy}}(w) = \sum_{l=0}^{G} \frac{H_l}{\Lambda_{xy}^{\beta_l} \Gamma(\beta_l)} w^{\beta_l - 1} e^{-\frac{w}{\Lambda_{xy}}} \quad \text{and} \quad \mathsf{F}_{g_{xy}}(w) = 1 - \sum_{l=0}^{G} \sum_{c=0}^{\beta_l - 1} \frac{H_l}{\Lambda_{xy}^{c} c!} w^{c} e^{-\frac{w}{\Lambda_{xy}}}, \tag{1}$$

whereby $\Lambda_{xy} = \frac{\vartheta_{xy}(\beta+\kappa\mu)}{\mu\beta(\kappa+1)}$, $H_l = \left(\frac{\kappa\mu}{\beta+\kappa\mu}\right)^{G-l} \left(\frac{\beta}{\beta+\kappa\mu}\right)^{l} \mathsf{C}_G^l$, $\beta_l = \beta - l$, $G = \beta - \mu$ with $\mu \leq \beta$. To represent path loss, we model ϑ_{xy} as $\varrho d_{xy}^{-\sigma}$ with ϱ being fading power at 1 meter (m), σ being path loss decay, d_{xy} being transceiver distance [7].

Independent and identically distributed (i.i.d) fading channels between the NOMA user i and PS's antennas are supposed and ergo, the subscripts $s_v i$ related to channel specifications ($g_{s_v i}$, $\Lambda_{s_v i}$, $\vartheta_{s_v i}$) can be written shortly as si in (g_{si}, Λ_{si}, ϑ_{si}) if not inducing any confusion, viz. $\epsilon_{s_v i} = \epsilon_{si}, \forall v, \epsilon = \{g, \Lambda, \vartheta\}$.

2.3. Signal representation

PS grants energy for U2 and U1 over multiple-input single-output links in Stage 1, considerably increasing amount of collected power at U2 and U1. Accordingly, the energy available at the NOMA user i is $E_i = \rho\alpha TP \sum_{v=1}^{V} g_{s_v i}$ where P is per-antenna power of PS, $g_{s_v i} = |h_{s_v i}|^2$ with $h_{s_v i}$ being channel gain between the NOMA user i and the v^{th} antenna of PS, and $\rho \in (0,1)$ means energy converting efficiency. Power available for Stage 2 transferred from E_i is $\frac{E_i}{(1-\alpha)T}$ due to Stage 2 prolonging $(1-\alpha)T$ time unit. Thereby, the NOMA user i conducts transmission in Stage 2 with the following power aligned with NLEH in [6]:

$$P_i = \begin{cases} \frac{\rho\alpha P}{1-\alpha} \sum_{v=1}^{V} g_{s_v i} & , \alpha P \sum_{v=1}^{V} g_{s_v i} \leq \psi \\ \frac{\rho\alpha\psi}{1-\alpha} & , \alpha P \sum_{v=1}^{V} g_{s_v i} > \psi \end{cases} = \begin{cases} AQ_i & , Q_i \leq B \\ D & , Q_i > B \end{cases} \tag{2}$$

wherein ψ is the power saturation threshold, $A = \frac{\rho\alpha P}{1-\alpha}$, $D = \frac{\rho\alpha\psi}{1-\alpha}$, $B = \frac{\psi}{\alpha P}$, and $Q_i = \sum_{v=1}^{V} g_{s_v i}$.

Stage 2 is for uplink communications using NOMA where U2 and U1 conduct concurrent transmissions of x_1 and x_2 with powers of P_1 and P_2 to NR where $\mathsf{E}\left\{|x_1|^2\right\} = \mathsf{E}\left\{|x_2|^2\right\} = 1$. Accordingly, NR receives a signal as

$$y = h_1\sqrt{P_1}x_1 + h_2\sqrt{P_2}x_2 + \xi, \tag{3}$$

wherein NR suffers the noise $\xi \sim \mathsf{N}(0, \zeta)$, h_1 and h_2 are channel gains correspondingly pertinent to channel power gains as $g_1 = |h_1|^2$ and $g_2 = |h_2|^2$.

Relied on (3), NR performs decoding x_1 and x_2 using NOMA principle. Two cases of the order to recover x_1 and x_2 are possible. If the signal from U1 is stronger than U2 ($g_1 P_1 > g_2 P_2$), then NR firsly recovers x_1 by behaving x_2 as noise. Thereby, NR restores x_1 with signal-to-interference plus noise ratio (SINR) derived from (3) as

$$\tilde{\gamma}^{x_1} = \frac{g_1 P_1}{g_2 P_2 + \zeta}. \tag{4}$$

After suppressing noise which x_1 generates, NR keeps recovering x_2 from $\tilde{y} = y - h_1\sqrt{P_1}x_1 = h_2\sqrt{P_2}x_2 + \xi$. Accordingly, in line with $\tilde{y}$, NR recovers x_2 with signal-to-noise ratio (SNR) to be

$$\tilde{\gamma}^{x_2} = \frac{g_2 P_2}{\zeta}. \tag{5}$$

Similarly, if the signal from U2 is stronger than U1 ($g_2P_2 > g_1P_1$), then NR firstly recovers x_2 under consideration of x_1 with the role of noise. Afterwards, NR decodes x_2 with SINR derived by (3) as

$$\hat{\gamma}^{x_2} = \frac{g_2 P_2}{g_1 P_1 + \zeta}. \tag{6}$$

Subsequently after suppressing noise that x_2 induces, NR keeps recovering x_1 from $\hat{y} = y - h_2\sqrt{P_2}x_2 = h_1\sqrt{P_1}x_1 + \xi$. Thereby, in line with $\hat{y}$, NR decodes x_1 with SNR to be

$$\hat{\gamma}^{x_1} = \frac{g_1 P_1}{\zeta}. \tag{7}$$

3. PERFORMANCE ANALYSIS OF ENOMAU

This part initially makes the OP analysis of eNOMAu. The OP stands for the probability which the channel capacity lowers the predetermined transmission speed C_0. Thereafter, OP analysis is reused to attain TP analysis. Such analyses offer prompt TP/OP assessment irrespective of exhaustive simulations.

3.1. OP of U1

There are three scenarios that cause U1 to be in outage:

- The 1st scenario is when the signal at NR from U1 is stronger than that from U2 ($g_1P_1 > g_2P_2$) and NR fails to decode x_1 ($\tilde{\gamma}^{x_1} < \gamma_0$) where $\gamma_0 = 2^{C_0/(1-\alpha)} - 1$.
- The 2nd scenario is when the signal at NR from U2 is stronger than that from U1 ($g_2P_2 > g_1P_1$) and NR fails to decode x_2 ($\hat{\gamma}^{x_2} < \gamma_0$).
- The 3rd scenario is when the signal at NR from U2 is stronger than that from U1 ($g_2P_2 > g_1P_1$) and NR decodes x_2 successfully ($\hat{\gamma}^{x_2} \geq \gamma_0$) but fails to decode x_1 ($\hat{\gamma}^{x_1} < \gamma_0$).

The OP of U1 is thereby expressed as:

$$\Upsilon_1 = \underbrace{\Pr\left\{g_1P_1 > g_2P_2, \tilde{\gamma}^{x_1} < \gamma_0\right\}}_{\Upsilon_{11}} + \underbrace{\Pr\left\{g_1P_1 < g_2P_2, \hat{\gamma}^{x_2} < \gamma_0\right\}}_{\Upsilon_{12}} + \underbrace{\Pr\left\{g_1P_1 < g_2P_2, \hat{\gamma}^{x_2} \geq \gamma_0, \hat{\gamma}^{x_1} < \gamma_0\right\}}_{\Upsilon_{13}}. \tag{8}$$

Now, we derive all terms (Υ_{11}, Υ_{12}, Υ_{13}) to complete the derivation of (8). First, inserting (4) into (8) yields.

$$\begin{aligned}
\Upsilon_{11} &= \Pr\left\{g_1P_1 > g_2P_2, \frac{g_1P_1}{g_2P_2+\zeta} < \gamma_0\right\} \\
&= \Pr\left\{z_1 > z_2, z_1 < \gamma_0 z_2 + \gamma_0\zeta\right\} \\
&= \Pr\left\{z_2 < z_1 < \gamma_0 z_2 + \gamma_0\zeta, z_2 < \gamma_0 z_2 + \gamma_0\zeta\right\} \\
&= \begin{cases} \overbrace{\Pr\left\{z_2 < z_1 < \gamma_0 z_2 + \gamma_0\zeta\right\}}^{\tilde{\Upsilon}_{11}} & ,\gamma_0 \geq 1 \\ \underbrace{\Pr\left\{z_2 < z_1 < \gamma_0 z_2 + \gamma_0\zeta, z_2 < \frac{\gamma_0\zeta}{1-\gamma_0}\right\}}_{\tilde{\Upsilon}_{12}} & ,\gamma_0 < 1 \end{cases}
\end{aligned} \tag{9}$$

where $z_1 = g_1P_1$ and $z_2 = g_2P_2$.

Comment 1: One sees from (9) that since $\gamma_0 = 2^{C_0/(1-\alpha)} - 1$, selecting the target spectral efficiency C_0 and the time portion α leads to $\gamma_0 < 1$ or $\gamma_0 \geq 1$, inducing Υ_{11} to accept different values and eventually causing different outage levels for U1. Also, since $\tilde{\Upsilon}_{11} > \tilde{\Upsilon}_{12}$ and γ_0 represents the SNR/SINR threshold, Υ_{11} when selecting C_0 and α in order for γ_0 to be large (i.e. $\gamma_0 \geq 1$) is larger than that when selecting C_0 and α in order for γ_0 to be small (i.e. $\gamma_0 < 1$).

$\tilde{\Upsilon}_{11}$ and $\tilde{\Upsilon}_{12}$ are represented through $\mathsf{f}_{z_2}(\cdot)$ and $\mathsf{F}_{z_1}(\cdot)$ as follows:

$$\tilde{\Upsilon}_{11} = \int_0^{\infty} \left[\mathsf{F}_{z_1}(\gamma_0 x + \gamma_0 \zeta) - \mathsf{F}_{z_1}(x)\right] \mathsf{f}_{z_2}(x) dx, \ \ \tilde{\Upsilon}_{12} = \int_0^{\frac{\gamma_0 \zeta}{1-\gamma_0}} \left[\mathsf{F}_{z_1}(\gamma_0 x + \gamma_0 \zeta) - \mathsf{F}_{z_1}(x)\right] \mathsf{f}_{z_2}(x) dx, \tag{10}$$

where the CDF of z_i, $i = \{1, 2\}$, is proved in [31] as:

$$\mathsf{F}_{z_i}(x) = \frac{B}{2} \sum_{u=1}^{U} \frac{\pi}{U} \sqrt{1-\varphi_u^2} \mathsf{f}_{Q_i}(\varpi_u) \mathsf{F}_{g_i}\left(\frac{x}{A\varpi_u}\right) + \bar{\mathsf{F}}_{Q_i}(B) \mathsf{F}_{g_i}\left(\frac{x}{D}\right), \tag{11}$$

wherein U is a parameter of Gaussian-Chebyshev quadrature [32], $\varpi_u = \frac{B}{2}(\varphi_u + 1)$, and $\varphi_u = \cos\left(\frac{2u-1}{2U}\pi\right)$. Moreover, [31] showed $\mathsf{f}_{Q_i}(x)$ and $\bar{\mathsf{F}}_{Q_i}(x)$ as:

$$\mathsf{f}_{Q_i}(x) = \sum_{\sum_{v=0}^{G} a_v = V} V! \left\{\prod_{t=0}^{G} \frac{(H_t)^{a_t}}{a_t!}\right\} \frac{x^{\phi-1}}{\Lambda_{si}^{\phi}\Gamma(\phi)} e^{-\frac{x}{\Lambda_{si}}}, \ \ \bar{\mathsf{F}}_{Q_i}(x) = \sum_{\sum_{v=0}^{G} a_v = V} \Gamma\left(\phi, \frac{x}{\Lambda_{si}}\right) \frac{V!}{\Gamma(\phi)} \prod_{t=0}^{G} \frac{(H_t)^{a_t}}{a_t!}, \tag{12}$$

where $\phi = \sum_{t=0}^{G} a_t \beta_t$.

The derivative of $\mathsf{F}_{z_i}(x)$ yeilds the PDF of z_i to be:

$$\mathsf{f}_{z_i}(x) = \frac{d\mathsf{F}_{z_i}(x)}{dx} = \frac{B}{2} \sum_{u=1}^{U} \sqrt{1-\varphi_u^2} \frac{\pi \mathsf{f}_{Q_i}(\varpi_u)}{UA\varpi_u} \mathsf{f}_{g_i}\left(\frac{x}{A\varpi_u}\right) + \frac{\bar{\mathsf{F}}_{Q_i}(B)}{D} \mathsf{f}_{g_i}\left(\frac{x}{D}\right). \tag{13}$$

Inserting (11) and (13) into (10) and after some careful simplifications, one attains the explicit expression of $\tilde{\Upsilon}_{11}$ to be:

$$\begin{aligned}\tilde{\Upsilon}_{11} = {} & \frac{\bar{\mathsf{F}}_{Q_1}(B) \bar{\mathsf{F}}_{Q_2}(B)}{D} \Psi(D, D) + \frac{\pi B}{2U} \sum_{u=1}^{U} \sqrt{1-\varphi_u^2} \left\{ \frac{\mathsf{f}_{Q_1}(\varpi_u) \bar{\mathsf{F}}_{Q_2}(B)}{D} \Psi(A\varpi_u, D) + \right. \\ & \left. \frac{\mathsf{f}_{Q_2}(\varpi_u) \bar{\mathsf{F}}_{Q_1}(B)}{A\varpi_u} \Psi(D, A\varpi_u) + \frac{\pi B}{2U} \sum_{v=1}^{U} \sqrt{1-\varphi_v^2} \frac{\mathsf{f}_{Q_1}(\varpi_u) \mathsf{f}_{Q_2}(\varpi_v)}{\varpi_v A} \Psi(A\varpi_u, A\varpi_v) \right\},\end{aligned} \tag{14}$$

where φ_v and ϖ_v are defined in the same manner as φ_u and ϖ_u whilst the function $\Psi(\cdot,\cdot)$ has a closed form as (17).

$\Psi(\cdot,\cdot)$ is a function of two arguments (I, J) as:

$$\Psi(I, J) = \int_0^{\infty} \left[\mathsf{F}_{g_1}\left(\frac{\gamma_0 x + \gamma_0 \zeta}{I}\right) - \mathsf{F}_{g_1}\left(\frac{x}{I}\right)\right] \mathsf{f}_{g_2}\left(\frac{x}{J}\right) dx. \tag{15}$$

Invoking $\mathsf{f}_{g_i}(\cdot)$ and $\mathsf{F}_{g_i}(\cdot)$ in (1) and using the binomial expansion, one simplifies $\Psi(I,J)$ as:

$$\begin{aligned}
\Psi(I,J) &= \int_0^\infty \left[\sum_{k=0}^{G}\sum_{u=0}^{\beta_k-1}\frac{H_k}{(\Lambda_1 I)^u u!}\left(x^u e^{-\frac{x}{\Lambda_1 I}} - e^{-\frac{\gamma_0\zeta}{\Lambda_1 I}}\gamma_0^u (x+\zeta)^u e^{-\frac{\gamma_0 x}{\Lambda_1 I}}\right)\right]\times \\
&\left[\sum_{m=0}^{G}\frac{H_m J^{1-\beta_m}}{\Lambda_2^{\beta_m}\Gamma(\beta_m)}x^{\beta_m-1}e^{-\frac{x}{\Lambda_2 J}}\right]dx \\
&= \sum_{k=0}^{G}\sum_{u=0}^{\beta_k-1}\sum_{m=0}^{G}\frac{H_k H_m J^{1-\beta_m}}{(\Lambda_1 I)^u u!\Lambda_2^{\beta_m}\Gamma(\beta_m)}\int_0^\infty\left[x^{u+\beta_m-1}e^{-\left(\frac{1}{\Lambda_1 I}+\frac{1}{\Lambda_2 J}\right)x} - \right. \\
&\left. e^{-\frac{\gamma_0\zeta}{\Lambda_1 I}}\gamma_0^u e^{-\left(\frac{\gamma_0}{\Lambda_1 I}+\frac{1}{\Lambda_2 J}\right)x}x^{\beta_m-1}\sum_{l=0}^{u}\mathsf{C}_u^l x^l\zeta^{u-l}\right]dx \\
&= \sum_{k=0}^{G}\sum_{u=0}^{\beta_k-1}\sum_{m=0}^{G}\frac{H_k H_m J^{1-\beta_m}}{(\Lambda_1 I)^u u!\Lambda_2^{\beta_m}\Gamma(\beta_m)}\left[\int_0^\infty x^{u+\beta_m-1}e^{-\left(\frac{1}{\Lambda_1 I}+\frac{1}{\Lambda_2 J}\right)x}dx - \right. \\
&\left. e^{-\frac{\gamma_0\zeta}{\Lambda_1 I}}\gamma_0^u\sum_{l=0}^{u}\mathsf{C}_u^l\zeta^{u-l}\int_0^\infty x^{l+\beta_m-1}e^{-\left(\frac{\gamma_0}{\Lambda_1 I}+\frac{1}{\Lambda_2 J}\right)x}dx\right].
\end{aligned} \tag{16}$$

The last integrals in (16) are solved with the help of [33] (3.351.3) Grad, eventually leading to the closed form of $\Psi(I,J)$ as:

$$\begin{aligned}
\Psi(I,J) = \sum_{m=0}^{G}\sum_{k=0}^{G}\sum_{u=0}^{\beta_k-1}\frac{H_k H_m J^{1-\beta_m}}{(\Lambda_1 I)^u u!\Lambda_2^{\beta_m}\Gamma(\beta_m)}&\left[\Gamma(u+\beta_m)\left(\frac{1}{\Lambda_1 I}+\frac{1}{\Lambda_2 J}\right)^{-(u+\beta_m)} - \right. \\
&\left. e^{-\frac{\gamma_0\zeta}{\Lambda_1 I}}\gamma_0^u\sum_{l=0}^{u}C_u^l\zeta^{u-l}\Gamma(l+\beta_m)\left(\frac{\gamma_0}{\Lambda_1 I}+\frac{1}{\Lambda_2 J}\right)^{-(l+\beta_m)}\right].
\end{aligned} \tag{17}$$

Subsequently, by exploiting the Gaussian-Chebyshev quadrature, one tightly approximates $\tilde{\Upsilon}_{12}$ as:

$$\tilde{\Upsilon}_{12} = \frac{\gamma_0\zeta}{2(1-\gamma_0)}\sum_{u=1}^{U}\frac{\pi}{U}\sqrt{1-\varphi_u^2}\left[\mathsf{F}_{z_1}(\gamma_0\chi_u+\gamma_0\zeta) - \mathsf{F}_{z_1}(\chi_u)\right]\mathsf{f}_{z_2}(\chi_u), \tag{18}$$

where $\chi_u = \frac{\gamma_0\zeta}{2(1-\gamma_0)}(\varphi_u+1)$.

Next, inserting $\hat{\gamma}^{x_2}$ in (6) into Υ_{12} yields.

$$\Upsilon_{12} = \Pr\left\{g_1P_1 < g_2P_2, \frac{g_2P_2}{g_1P_1+\zeta} < \gamma_0\right\}. \tag{19}$$

By comparing Υ_{12} in (19) with Υ_{11} in (9), one recognizes that the explicit formula of Υ_{12} is obtained from that of Υ_{11} by interchanging $(\Lambda_1, \Lambda_{s1})$ and $(\Lambda_2, \Lambda_{s2})$. Accordingly, the derivation of Υ_{12} is omitted for compactness.

Finally, inserting $\hat{\gamma}^{x_2}$ in (6) and $\hat{\gamma}^{x_1}$ in (7) into Υ_{13} yields.

$$\begin{aligned}
\Upsilon_{13} &= \Pr\left\{g_1P_1 < g_2P_2, \frac{g_2P_2}{g_1P_1+\zeta} \ge \gamma_0, \frac{g_1P_1}{\zeta} < \gamma_0\right\} \\
&= \Pr\left\{g_1P_1 < g_2P_2, g_2P_2 \ge \gamma_0 g_1P_1 + \gamma_0\zeta, g_1P_1 < \gamma_0\zeta\right\} \\
&= \Pr\left\{g_2P_2 \ge \gamma_0 g_1P_1 + \gamma_0\zeta, g_1P_1 < \gamma_0\zeta\right\} \\
&= \int_0^{\gamma_0\zeta}\left[1 - \mathsf{F}_{z_2}(\gamma_0 x + \gamma_0\zeta)\right]\mathsf{f}_{z_1}(x)dx \\
&= \mathsf{F}_{z_1}(\gamma_0\zeta) - \int_0^{\gamma_0\zeta}\mathsf{F}_{z_2}(\gamma_0 x + \gamma_0\zeta)\,\mathsf{f}_{z_1}(x)dx.
\end{aligned} \tag{20}$$

$\int_0^{\gamma_0\zeta} \mathsf{F}_{z_2}(\gamma_0 x + \gamma_0\zeta)\, \mathsf{f}_{z_1}(x)dx$ has a tight approximation by employing Gaussian-Chebyshev quadrature, yielding.

$$\Upsilon_{13} = \mathsf{F}_{z_1}(\gamma_0\zeta) - \frac{\gamma_0\zeta}{2}\sum_{u=1}^{U}\frac{\pi}{U}\sqrt{1-\varphi_u^2}\mathsf{F}_{z_2}(\gamma_0\delta_u + \gamma_0\zeta)\, \mathsf{f}_{z_1}(\delta_u), \tag{21}$$

where $\delta_u = \frac{\gamma_0\zeta}{2}(\varphi_u + 1)$.

3.2. OP of U2

There are three scenarios that cause U2 to be in outage:

- The 1st scenario is when the signal at NR from U2 is stronger than that from U1 ($g_2P_2 > g_1P_1$) and NR fails to decode x_2 ($\hat{\gamma}^{x_2} < \gamma_0$).
- The 2nd scenario is when the signal at NR from U1 is stronger than that from U2 ($g_1P_1 > g_2P_2$) and NR fails to decode x_1 ($\tilde{\gamma}^{x_1} < \gamma_0$).
- The 3rd scenario is when the signal at NR from U1 is stronger than that from U2 ($g_1P_1 > g_2P_2$) and NR decodes x_1 successfully ($\tilde{\gamma}^{x_1} \geq \gamma_0$) yet fails to recover x_2 ($\tilde{\gamma}^{x_2} < \gamma_0$).

The OP of U2 is thereby expressed as:

$$\Upsilon_2 = \underbrace{\Pr\left\{g_1P_1 < g_2P_2, \hat{\gamma}^{x_2} < \gamma_0\right\}}_{\Upsilon_{21}} + \underbrace{\Pr\left\{g_1P_1 > g_2P_2, \tilde{\gamma}^{x_1} < \gamma_0\right\}}_{\Upsilon_{22}} + \underbrace{\Pr\left\{g_1P_1 > g_2P_2, \tilde{\gamma}^{x_1} \geq \gamma_0, \tilde{\gamma}^{x_2} < \gamma_0\right\}}_{\Upsilon_{23}}. \tag{22}$$

By comparing (22) with (8), one infers that $\Upsilon_{21} = \Upsilon_{12}$ and $\Upsilon_{22} = \Upsilon_{11}$. Moreover, inserting $\tilde{\gamma}^{x_1}$ in (4) and $\tilde{\gamma}^{x_2}$ in (5) into (22) yields.

$$\Upsilon_{23} = \Pr\left\{g_1P_1 > g_2P_2, \frac{g_1P_1}{g_2P_2 + \zeta} \geq \gamma_0, \frac{g_2P_2}{\zeta} < \gamma_0\right\}. \tag{23}$$

By comparing Υ_{23} with Υ_{13} in (20), one recognizes that the explicit formula of Υ_{23} is obtained from that of Υ_{13} by interchanging $(\Lambda_1, \Lambda_{s1})$ and $(\Lambda_2, \Lambda_{s2})$. Accordingly, the derivations of Υ_{21}, Υ_{22}, and Υ_{23} are omitted for compactness. Moreover, similar to Υ_1, one sees that the outage level of U2, Υ_2, can be adjusted by selecting properly C_0 and α.

Comment 2: Both Υ_1 and Υ_2 are functions of specifications (C_0, α, P, V, ψ, ρ). This implies U1 and U2 is able to attain target performances by properly choosing these specifications.

3.3. Throughput

In delay-constrained communication, the throughput of Ui for eNOMAu is computed as:

$$\Delta_i = (1-\alpha)C_0(1-\Upsilon_i). \tag{24}$$

One sees from (24) that the TP of Ui is jointly specified by parameters (C_0, α, P, V, ψ, ρ) since this cluster impacts Υ_i. Accordingly, the expected TP is obtained by appropriately choosing such parameters based on their preset value ranges.

4. ASYMPTOTIC ANALYSIS OF ENOMAU

This section studies the performance upper-bound of eNOMAu corresponding to high transmission power ($P \to \infty$). In such a regime, energy harvester definitely saturates and ergo, $P_i \to D$ with $i = \{1, 2\}$. Accordingly, the CDF and PDF of $z_i = g_iD$ reduce to $\mathsf{F}_{z_i}(x) = \mathsf{F}_{g_i}\left(\frac{x}{D}\right)$ and $\mathsf{f}_{z_i}(x) = \frac{1}{D}\mathsf{f}_{g_i}\left(\frac{x}{D}\right)$, correspondingly, when $P \to \infty$. Therefore, the OP of Ui is summarized to be:

$$\Upsilon_i^{\infty} = \Upsilon_{i1}^{\infty} + \Upsilon_{i2}^{\infty} + \Upsilon_{i3}^{\infty}, \tag{25}$$

where $\Upsilon_{11}^{\infty} = \Upsilon_{22}^{\infty}$, $\Upsilon_{12}^{\infty} = \Upsilon_{21}^{\infty}$, the explicit expressions of Υ_{12}^{∞} and Υ_{23}^{∞} are obtained from those of Υ_{11}^{∞} and Υ_{13}^{∞} by interchanging $(\Lambda_1, \Lambda_{s1})$ and $(\Lambda_2, \Lambda_{s2})$, and

$$\Upsilon_{11}^{\infty} = \begin{cases} \tilde{\Upsilon}_{11}^{\infty} & , \gamma_0 \geq 1 \\ \tilde{\Upsilon}_{12}^{\infty} & , \gamma_0 < 1 \end{cases} \tag{26}$$

with

$$\tilde{\Upsilon}_{11}^{\infty}=\sum_{k=0}^{G}\sum_{u=0}^{\beta_k-1}\sum_{m=0}^{G}\frac{H_kH_mD^{-u-\beta_m}}{\Lambda_1^u u!\Lambda_2^{\beta_m}\Gamma(\beta_m)}\left[\Gamma(u+\beta_m)\left\{\left(\frac{1}{\Lambda_1}+\frac{1}{\Lambda_2}\right)\frac{1}{D}\right\}^{-u-\beta_m}-\right.$$
$$\left.e^{-\frac{\gamma_0\zeta}{\Lambda_1 D}}\gamma_0^u\sum_{l=0}^{u}\mathsf{C}_u^l\zeta^{u-l}\Gamma(l+\beta_m)\left\{\left(\frac{\gamma_0}{\Lambda_1}+\frac{1}{\Lambda_2}\right)\frac{1}{D}\right\}^{-l-\beta_m}\right] \tag{27}$$

$$\tilde{\Upsilon}_{12}^{\infty}=\sum_{k=0}^{G}\sum_{u=0}^{\beta_k-1}\sum_{m=0}^{G}\frac{H_kH_mD^{-u-\beta_m}}{\Lambda_1^u u!\Lambda_2^{\beta_m}\Gamma(\beta_m)}\left[\Phi\left(\frac{\gamma_0\zeta}{1-\gamma_0},u+\beta_m-1,\left[\frac{1}{\Lambda_1}+\frac{1}{\Lambda_2}\right]\frac{1}{D}\right)-\right.$$
$$\left.e^{-\frac{\gamma_0\zeta}{\Lambda_1 D}}\gamma_0^u\sum_{l=0}^{u}\mathsf{C}_u^l\zeta^{u-l}\Phi\left(\frac{\gamma_0\zeta}{1-\gamma_0},l+\beta_m-1,\left[\frac{\gamma_0}{\Lambda_1}+\frac{1}{\Lambda_2}\right]\frac{1}{D}\right)\right] \tag{28}$$

$$\tilde{\Delta}_{13}^{\infty}=\sum_{k=0}^{G}\sum_{u=0}^{\beta_k-1}\sum_{m=0}^{G}\sum_{l=0}^{u}\frac{\mathsf{C}_u^l\Lambda_1^{-\beta_m}\zeta^{u-l}H_mH_k}{\Gamma(\beta_m)u!D^{u+\beta_m+1}}\left(\frac{\gamma_0}{\Lambda_2}\right)^u e^{-\frac{\gamma_0\zeta}{\Lambda_2 D}}\Phi\left(\gamma_0\zeta,l+\beta_m-1,\left[\frac{\gamma_0}{\Lambda_2}+\frac{1}{\Lambda_1}\right]\frac{1}{D}\right) \tag{29}$$

$$\Phi(a,b,c)=\frac{b!}{c^{b+1}}-e^{-ac}\sum_{v=0}^{b}\frac{b!}{v!}\frac{a^v}{c^{b-v+1}}. \tag{30}$$

5. ENERGY SCAVENGING-AIDED ORTHOGONAL MULTIPLE ACCESS UPLINK COMMUNICATIONS (EOMAU)

In energy scavenging-aided orthogonal multiple access uplink communications (eOMAu), Stage 2 is separated equally into two sub-stages during which U1 and U2 transmit their information sequentially and directly to NR. Therefore, NR receives the signal from Ui as $y_i = h_i\sqrt{P_i} + \xi_i$ where ξ_i is the noise at NR and $i = \{1, 2\}$. Accordingly, the channel capacity that Ui achieves is $\mathsf{R}_i = \frac{1-\alpha}{2}\log_2\left(1 + \frac{g_iP_i}{\zeta}\right)$ where the factor $\frac{1-\alpha}{2}$ before the logarithm is since Ui transmits only in $\frac{1-\alpha}{2}T$. Consequently, the OP of Ui is:

$$\Upsilon_i^{OMA}=\Pr\{\mathsf{R}_i<C_0\}=\Pr\left\{\frac{g_iP_i}{\zeta}<\tilde{\gamma}_0\right\}=\mathsf{F}_{z_i}(\tilde{\gamma}_0\zeta), \tag{31}$$

where $\tilde{\gamma}_0 = 2^{2C_0/(1-\alpha)} - 1$.

One notes that eOMAu is deemed as a baseline transmission scheme as compared to eNOMAu. Given the closed-form formula of Υ_i^{OMA}, it is convenient in quickly comparing the performances between eOMAu and eNOMAu from which the advantages of NOMA are exposed promptly.

6. EVALUATIONS

This section discusses multiple analytical/simulated findings to rate outage probabilities of U1 and U2 in eNOMAu and its eOMAu counterpart. The analytical formulas derived in sections 3-5 yield analytical findings (Ana.). Also, Monte-Carlo simulation is run, yielding simulated findings (Sim.). Comparing 'Sim.' with 'Ana.' validates theoretical derivations. Since OP and TP are linearly proportional to each other, TP is an one-by-one mapping of OP. Accordingly, this section presents merely outage probabilities of U1 and U2.

Terminals's positions are illustrated as NR $(50, 0)$ m, U1 $(0, 0)$ m, U2 $(-10, 15)$ m, PS $(-15, 0)$ m. Unless otherwise addressed, parameters are adopted as $(\kappa, \beta, \mu) = (3, 4, 2)$, $\varrho = 10^{-2}$, $\psi = -10$ dB, $\alpha = 0.4$, $\sigma = 3$, $P = 15$ dB, $C_0 = 0.5$ bps/Hz, $\rho = 0.7$, $V = 4$, and $\zeta = -90$ dBm. Findings in subsequent figures demonstrate that $i)$ analysis matches simulation, confirming preciseness of expressions obtained in sections 3-5; $ii)$ U1 outperforms U2, which makes sense since U1 is nearer to PS and NR than U2.

Figure 2(a) demonstrates OPs of U1 and U2 versus P, which unveils performance enhancement with accreting P for both U1 and U2. This makes sense owing to increasing scavenged energy. Further, eNOMAu significantly outperforms its eOMAu counterpart over the whole range of P, which exposes the advantage of NOMA in comparison with OMA. Also, Figure 2(b) reveals outage performances of U1 and U2 versus ψ. One recognizes that the performances of both U1 and U2 are ameliorated with accreting ψ, as anticipated, for both eNOMAu and eOMAu. Moreover, U1 and U2 saturate at high ψ because NLEH coincides LEH. Further, U1 and U2 are in a complete outage for low ψ, as anticipated. Furthermore, similar to Figure 2(a), findings in Figure 2(b) illustrate that eNOMAu considerably outperforms eOMAu for any ψ.

Figure 3 exposes OPs of U1 and U2 against V (Figure 3(a)) and ρ (Figure 3(b)). One expects that accreting V and ρ facilitates U1 and U2 in harvesting more energy and as a result, mitigating OPs of both U1 and U2. Figure 3 unveils exactly such an expectation wherein accreting V and ρ dramatically improves performances of both U1 and U2. Further, similar to Figure 2, the results in Figure 3 illustrate that eNOMAu is superior to its eOMAu counterpart over the whole range of V and ρ, which again illustrates the advantage of NOMA as compared to OMA.

Figure 4 reveals outage performances of U1 and U2 versus α (Figure 4(a)) and C_0 (Figure 4(b)). One observes from Figure 4(a) that one can optimize α to reach minimum OPs for U1 and U2, and for eNOMAu and eOMAu. The optimal α is for poising durations for ES and transmission. Additionally, Figure 4(b) illustrates outage increase with increasing C_0 for both U1 and U2 as well as both eNOMAu and eOMAu, as expected. As analyzed in section 3., the SNR/SINR threshold γ_0 is controlled jointly by C_0 and α. Moreover, the analysis in section 3 exposes that $\gamma_0 \geq 1$ and $\gamma_0 < 1$ cause different outage levels for eNOMAu. As such, the results in Figure 4(a) and Figure 4(b) make sense in that eNOMAu is not always better than eOMAu. More specifically, Figure 4(a) unveils that the performance of U1 (or U2) in eNOMAu outperforms that in eOMAu when $\alpha < 0.47$ (or $\alpha < 0.53$) whilst Figure 4(b) illustrates that the performance of U2 in eNOMAu outperforms that in eOMAu for any C_0 but the performance of U1 in eNOMAu outperforms that in eOMAu only for $C_0 < 0.57$ bps/Hz or $C_0 > 1.29$ bps/Hz.

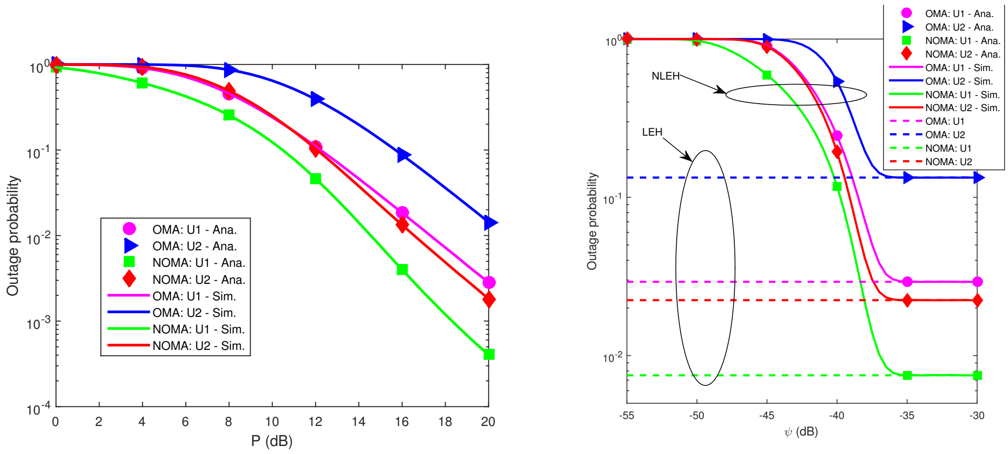

(a) (b)

Figure 2. Influence of (a) OP versus P and (b) OP versus ψ

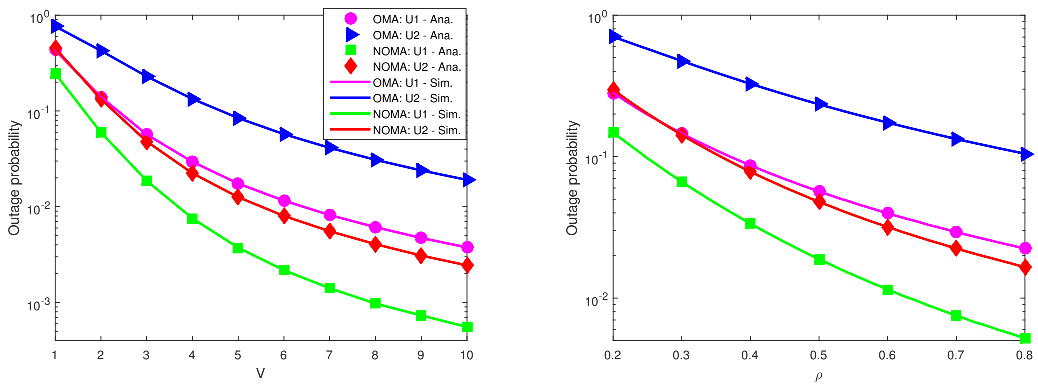

(a) (b)

Figure 3. Influence of (a) OP versus V and (b) OP versus ρ

$\kappa - \mu$ shadowed fading specified by parameters (κ, β, μ), which impact OPs of U1 and U2, are demonstrated in Figure 5 in which Figure 5(a) shows the impact of β while Figure 5(b) demonstrates the effect of κ. This figure reveals that the outage performances of U1 and U2 are ameliorated with accreting (β, κ, μ), as expected, for both eNOMAu and eOMAu. Interestingly, the performance improvement of eNOMAu with increasing μ is considerably higher than that of eOMAu, showing the dominance of NOMA to OMA when channels are less severe (i.e., μ increases).

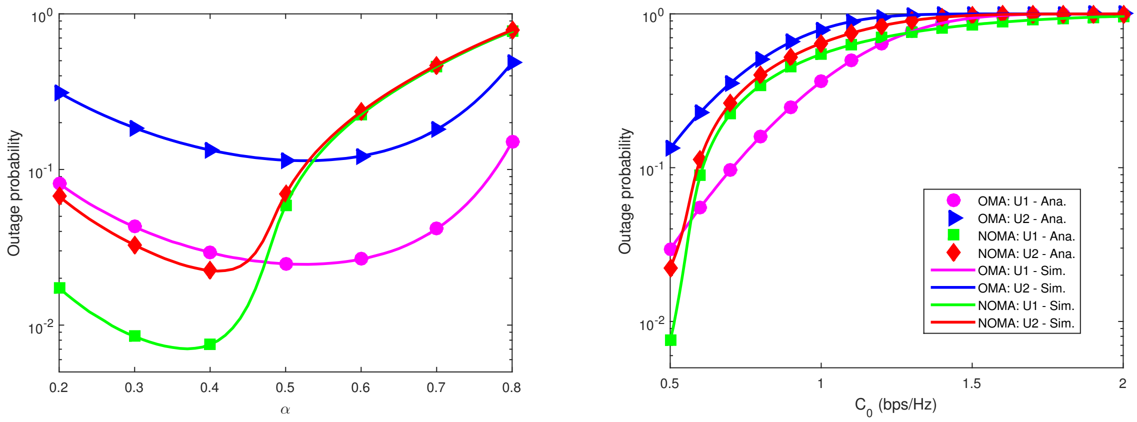

(a) (b)

Figure 4. Influence of (a) OP versus α and (b) OP versus C_0

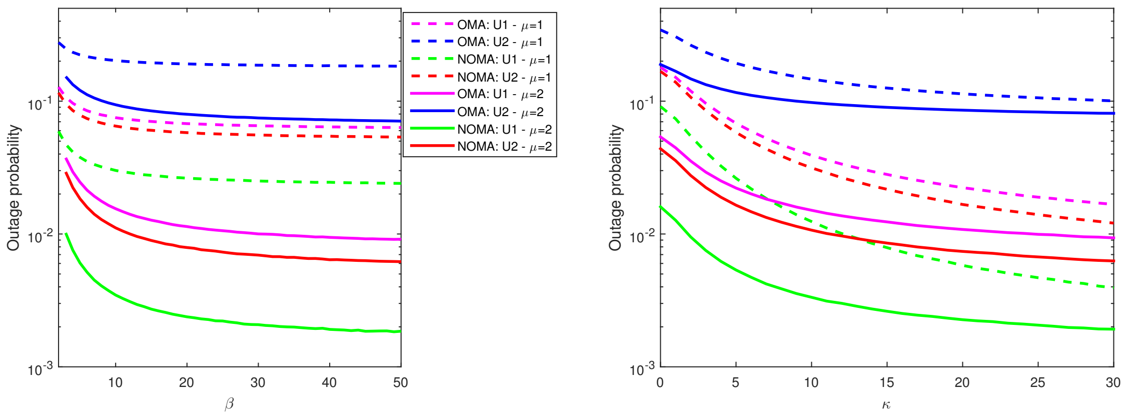

(a) (b)

Figure 5. Influence of (a) OP versus β and (b) OP versus κ

7. CONCLUSION

The paper analyzed the TP/OP of the suggested eNOMAu considering realistic operation conditions (multiple antennas, shadowing, NLEH, fading, path loss). The proposed analysis provides the explicit expressions that revealed directly complete comprehension of the proposed eNOMAu and rated system performance quickly in multiple sets of pivotal specifications. A multitude of findings revealed that ES nonlinearity drastically deteriorates system performance. Moreover, am expected performance can be reached by appropriately adopting specifications $(C_0, \alpha, P, V, \psi, \rho)$. Remarkably, eNOMAu attains optimum performance by properly selecting α. Furthermore, the performance of eNOMAu is dramatically enhanced with accreting V and better channel conditions. Moreover, eNOMAu is significantly superior to its eOMAu counterpart.

ACKNOWLEDGMENT

Khuong Ho-Van would like to thank Ho Chi Minh City University of Technology (HCMUT), VNU-HCM for the support of time and facilities for this study.

FUNDING INFORMATION

Authors state no funding involved.

AUTHOR CONTRIBUTIONS STATEMENT

This journal uses the Contributor Roles Taxonomy (CRediT) to recognize individual author contributions, reduce authorship disputes, and facilitate collaboration.

Name of Author	C	M	So	Va	Fo	I	R	D	O	E	Vi	Su	P	Fu
Huu Q. Tran	✓	✓		✓	✓	✓		✓	✓					
Khuong Ho-Van		✓				✓		✓		✓		✓		

C	: **C**onceptualization	I	: **I**nvestigation	Vi	: **Vi**sualization
M	: **M**ethodology	R	: **R**esources	Su	: **Su**pervision
So	: **So**ftware	D	: **D**ata Curation	P	: **P**roject Administration
Va	: **Va**lidation	O	: Writing - **O**riginal Draft	Fu	: **Fu**nding Acquisition
Fo	: **Fo**rmal Analysis	E	: Writing - Review & **E**diting		

CONFLICTS OF INTEREST

The authors declare no conflict of interest in this manuscript.

INFORMED CONSENT

We have obtained informed consent from all individuals included in this study.

ETHICAL APPROVAL

Not applicable.

DATA AVAILABILITY

Data availability is not applicable to this paper as no new data were created or analyzed in this study.

REFERENCES

[1] C. Zhang *et al.*, "Privacy-Preserving Federated Learning for Data Heterogeneity in 6G Mobile Networks," *IEEE Network*, vol. 39, no. 2, pp. 134–141, Mar. 2024, doi: 10.1109/MNET.2024.3510427.

[2] X. Lv, S. Rani, S. Manimurugan, A. Slowik, and Y. Feng, "Quantum-Inspired Sensitive Data Measurement and Secure Transmission in 5G-Enabled Healthcare Systems," *Tsinghua Science and Technology*, vol. 30, no. 1, pp. 456–478, Feb. 2025, doi: 10.26599/TST.2024.9010122.

[3] D. Wang and S. Men, "Secure energy efficiency for NOMA based cognitive radio networks with nonlinear energy harvesting," *IEEE Access*, vol. 6, pp. 62707–62716, 2018, doi: 10.1109/ACCESS.2018.2876970.

[4] M. A. Halimi, T. Khan, Nasimuddin, A. A. Kishk, and Y. M. M. Antar, "Rectifier Circuits for RF Energy Harvesting and Wireless Power Transfer Applications: A Comprehensive Review Based on Operating Conditions," *IEEE Microwave Magazine*, vol. 24, no. 1, pp. 46–61, Jan. 2023, doi: 10.1109/MMM.2022.3211594.

[5] D. Wang, F. Zhou, and V. C. M. Leung, "Primary Privacy Preserving with Joint Wireless Power and Information Transfer for Cognitive Radio Networks," *IEEE Transactions on Cognitive Communications and Networking*, vol. 6, no. 2, pp. 683–693, Jun. 2020, doi: 10.1109/TCCN.2019.2952885.

[6] S. Solanki, P. K. Upadhyay, D. B. Da Costa, H. Ding, and J. M. Moualeu, "Performance Analysis of Piece-Wise Linear Model of Energy Harvesting-Based Multiuser Overlay Spectrum Sharing Networks," *IEEE Open Journal of the Communications Society*, vol. 1, pp. 1820–1836, 2020, doi: 10.1109/OJCOMS.2020.3038012.

[7] D. Wang, F. Rezaei, and C. Tellambura, "Performance Analysis and Resource Allocations for a WPCN with a New Nonlinear Energy Harvester Model," *IEEE Open Journal of the Communications Society*, vol. 1, pp. 1403–1424, 2020, doi: 10.1109/OJCOMS.2020.3022316.

[8] F. J. Lopez-Martinez, J. F. Paris, and J. M. Romero-Jerez, "The κ- μ Shadowed Fading Model With Integer Fading Parameters," *IEEE Transactions on Vehicular Technology*, vol. 66, no. 9, pp. 7653–7662, Sep. 2017, doi: 10.1109/TVT.2017.2678430.

[9] A. Khazali, D. Tarchi, M. G. Shayesteh, H. Kalbkhani, and A. Bozorgchenani, "Energy Efficient Uplink Transmission in Cooperative mmWave NOMA Networks With Wireless Power Transfer," *IEEE Transactions on Vehicular Technology*, vol. 71, no. 1, pp. 391–405, Jan. 2022, doi: 10.1109/TVT.2021.3124076.

[10] C. K. Singh, V. Singh, P. K. Upadhyay, and M. Lin, "Energy Harvesting in Overlay Cognitive NOMA Systems With Hardware Impairments," *IEEE Systems Journal*, vol. 16, no. 2, pp. 2648–2659, Jun. 2022, doi: 10.1109/JSYST.2021.3082552.

[11] A. K. Shukla, V. Singh, P. K. Upadhyay, A. Kumar, and J. M. Moualeu, "Performance Analysis of Energy Harvesting-Assisted Overlay Cognitive NOMA Systems with Incremental Relaying," *IEEE Open Journal of the Communications Society*, vol. 2, pp. 1558–1576, 2021, doi: 10.1109/OJCOMS.2021.3093671.

[12] Y. Liu, Y. Ye, H. Ding, F. Gao, and H. Yang, "Outage Performance Analysis for SWIPT-Based Incremental Cooperative NOMA Networks With Non-Linear Harvester," *IEEE Communications Letters*, vol. 24, no. 2, pp. 287–291, Feb. 2020, doi: 10.1109/LCOMM.2019.2955951.

[13] Q. N. Le, A. Yadav, N. P. Nguyen, O. A. Dobre, and R. Zhao, "Full-Duplex Non-Orthogonal Multiple Access Cooperative Overlay Spectrum-Sharing Networks with SWIPT," *IEEE Transactions on Green Communications and Networking*, vol. 5, no. 1, pp. 322–334, Mar. 2021, doi: 10.1109/TGCN.2020.3036026.

[14] X. Liu, Y. Guo, and T. S. Durrani, "Simultaneous Wireless Information and Power Transfer Based on Symbol Allocation for GFDM-NOMA Cooperative Communications," *IEEE Wireless Communications Letters*, vol. 11, no. 2, pp. 333–337, Feb. 2022, doi: 10.1109/LWC.2021.3127243.

[15] D. T. Do, A. T. Le, Y. Liu, and A. Jamalipour, "User grouping and energy harvesting in uav-noma system with af/df relaying," *IEEE Transactions on Vehicular Technology*, vol. 70, no. 11, pp. 11855–11868, Nov. 2021, doi: 10.1109/TVT.2021.3116101.

[16] K. Agrawal, M. F. Flanagan, and S. Prakriya, "NOMA with Battery-Assisted Energy Harvesting Full-Duplex Relay," *IEEE Transactions on Vehicular Technology*, vol. 69, no. 11, pp. 13952–13957, Nov. 2020, doi: 10.1109/TVT.2020.3021085.

[17] L. Ma, E. Li, and Q. Yang, "On the Performance of Full-Duplex Cooperative NOMA with Non-Linear EH," *IEEE Access*, vol. 9, pp. 145968–145976, 2021, doi: 10.1109/ACCESS.2021.3124090.

[18] V. Aswathi and A. V. Babu, "Outage and throughput analysis of full-duplex cooperative noma system with energy harvesting," *IEEE Transactions on Vehicular Technology*, vol. 70, no. 11, pp. 11648–11664, Nov. 2021, doi: 10.1109/TVT.2021.3112596.

[19] Q. Si, M. Jin, T. A. Tsiftsis, N. Zhao, and X. Wang, "Cooperative SM-Based NOMA Scheme with SWIPT," *IEEE Transactions on Vehicular Technology*, vol. 70, no. 6, pp. 6195–6199, Jun. 2021, doi: 10.1109/TVT.2021.3076565.

[20] C. E. Garcia, M. R. Camana, and I. Koo, "Low-Complexity PSO-Based Resource Allocation Scheme for Cooperative Non-Linear SWIPT-Enabled NOMA," *IEEE Access*, vol. 10, pp. 34207–34220, 2022, doi: 10.1109/ACCESS.2022.3162838.

[21] T. N. Tran, T. P. Vo, P. Fazio, and M. Voznak, "SWIPT Model Adopting a PS Framework to Aid IoT Networks Inspired by the Emerging Cooperative NOMA Technique," *IEEE Access*, vol. 9, pp. 61489–61512, 2021, doi: 10.1109/ACCESS.2021.3074351.

[22] X. Li et al., "Cooperative wireless-powered noma relaying for b5g iot networks with hardware impairments and channel estimation errors," *IEEE Internet of Things Journal*, vol. 8, no. 7, pp. 5453–5467, Apr. 2021, doi: 10.1109/JIOT.2020.3029754.

[23] S. Bisen, P. Shaik, and V. Bhatia, "On Performance of Energy Harvested Cooperative NOMA under Imperfect CSI and Imperfect SIC," *IEEE Transactions on Vehicular Technology*, vol. 70, no. 9, pp. 8993–9005, Sep. 2021, doi: 10.1109/TVT.2021.3099067.

[24] C. Zhai, Y. Li, X. Wang, and Z. Yu, "Nonorthogonal Multiple Access with Energy Harvesting-Based Alternate Relaying," *IEEE Systems Journal*, vol. 16, no. 1, pp. 327–338, Mar. 2022, doi: 10.1109/JSYST.2020.3034247.

[25] R. Lei, D. Xu, and I. Ahmad, "Secrecy Outage Performance Analysis of Cooperative NOMA Networks with SWIPT," *IEEE Wireless Communications Letters*, vol. 10, no. 7, pp. 1474–1478, Jul. 2021, doi: 10.1109/LWC.2021.3070429.

[26] X. Li, J. Li, and L. Li, "Performance Analysis of Impaired SWIPT NOMA Relaying Networks over Imperfect Weibull Channels," *IEEE Systems Journal*, vol. 14, no. 1, pp. 669–672, Mar. 2020, doi: 10.1109/JSYST.2019.2919654.

[27] M. Aldababsa and E. Basar, "Joint Transmit-and-Receive Antenna Selection System for MIMO-NOMA With Energy Harvesting," *IEEE Systems Journal*, vol. 16, no. 3, pp. 4139–4148, Sep. 2022, doi: 10.1109/JSYST.2021.3109306.

[28] B. Lyu, P. Ramezani, D. T. Hoang, and A. Jamalipour, "IRS-Assisted Downlink and Uplink NOMA in Wireless Powered Communication Networks," *IEEE Transactions on Vehicular Technology*, vol. 71, no. 1, pp. 1083–1088, Jan. 2022, doi: 10.1109/TVT.2021.3126013.

[29] Q. Wu, X. Zhou, and R. Schober, "IRS-Assisted Wireless Powered NOMA: Do We Really Need Different Phase Shifts in DL and UL?," *IEEE Wireless Communications Letters*, vol. 10, no. 7, pp. 1493–1497, Jul. 2021, doi: 10.1109/LWC.2021.3072502.

[30] D. Zhang, Q. Wu, M. Cui, G. Zhang, and D. Niyato, "Throughput Maximization for IRS-Assisted Wireless Powered Hybrid NOMA and TDMA," *IEEE Wireless Communications Letters*, vol. 10, no. 9, pp. 1944–1948, Sep. 2021, doi: 10.1109/LWC.2021.3087495.

[31] T. Le-Thanh and K. Ho-Van, "Performance Analysis of Wireless Communications with Nonlinear Energy Harvesting under Hardware Impairment and κ- μ Shadowed Fading," *Sensors*, vol. 23, no. 7, p. 3619, Mar. 2023, doi: 10.3390/s23073619.

[32] M. Abramowitz, I. A. Stegun, and J. E. Romain, Handbook of Mathematical Functions, with Formulas, Graphs, and Mathematical Tables. *Washington DC: U.S. Government Printing Office*, 1972.

[33] I. S. Gradshteyn, I. M. Ryzhik, A. Jeffrey, Y. V. Geronimus, M. Y. Tseytlin, and Y. C. Fung, Table of Integrals, Series, and Products, *6th ed. San Diego: CA: Academic*, 1981.

BIOGRAPHIES OF AUTHORS

Huu Q. Tran received the M.S degree in Electronics Engineering from Ho Chi Minh City University of Technology and Education (HCMUTE), Vietnam in 2010. Currently, he has been working as a lecturer at Faculty of Electronics Technology, Industrial University of Ho Chi Minh City (IUH), Vietnam. He obtained his doctorate from the Faculty of Electrical and Electronics Engineering at HCMUTE, Vietnam. His research interests include wireless communications, non-orthogonal multiple access (NOMA), energy harvesting (EH), wireless cooperative relaying networks, heterogeneous networks (HetNet), cloud radio access networks (C-RAN), unmanned aerial vehicles (UAV), reconfigurable intelligent surfaces (RIS), short-packet communication (SPC) and internet of things (IoT). He can be contacted at email: tranquyhuu@iuh.edu.vn.

Khuong Ho-Van received the B.E. (first-ranked honor) and M.S. degrees in Electronics and Telecommunications Engineering from Ho Chi Minh City University of Technology, Vietnam, in 2001 and 2003, respectively, and the Ph.D. degree in Electrical Engineering from the University of Ulsan, South Korea, in 2007. From 2007 to 2011, he joined McGill University, Canada, as a Postdoctoral Fellow. Currently, he is an Associate Professor with Ho Chi Minh City University of Technology, Vietnam. His major research interests include modulation and coding techniques, diversity techniques, digital signal processing, energy harvesting, physical layer security, and cognitive radio. He can be contacted at email: hvkhuong@hcmut.edu.vn.